THE JOURNAL OF PHYSICAL CHEMISTRY B

ARTICLE

pubs.acs.org/JPCB

Analysis of the Lamellar Structure of Semicrystalline Polymers by Direct Model Fitting of SAXS Patterns

Stefan Fischer, Zhiyong Jiang, and Yongfeng Men*

State Key Laboratory of Polymer Physics and Chemistry, Changchun Institute of Applied Chemistry, Renmin Street 5625, Changchun, P.R. China, 130022, People's Republic of China

Supporting Information

ABSTRACT: Small-angle X-ray scattering data of melt-drawn high-density polyethylene (HDPE) have been analyzed by direct model fitting to projections on the drawing direction. On the basis of the assumption of an infinite paracrystalline lattice as proposed by Hosemann and a rectangular density profile, several additional assumptions have been tested. It turned out that to achieve good fits we have to introduce a finiteness of the lattice for the used samples. Transition zones between crystalline and amorphous regions also improve the model but are of less importance. The most suitable model has been tested on data from an annealing and subsequent cooling process. We show that the additional parameters gained in the modeling approach compared to peak analysis or correlation function analysis lead to a better understanding of the structures and processes in the samples.

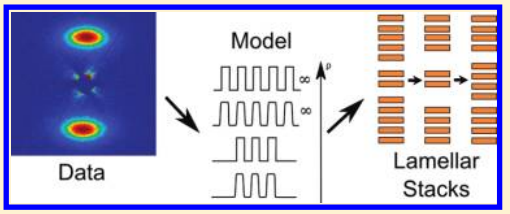

1. INTRODUCTION

Small-angle X-ray scattering (SAXS) technique is a versatile tool to analyze the bulk properties of semicrystalline polymers on the lamellar scale during processes such as thermal treatment or deformation of a solidified polymer.[1,2] In general, the scattering amplitude is the Fourier-transform of the electron density variation in the sample. Due to the loss of phase information during the recording process, a direct calculation of the structure from the scattering pattern is infeasible. Classical approaches to evaluate SAXS of semicrystalline polymers include peak analysis,[3,4] correlation function,[2,5,6] and interface distribution function (IDF).[7−9] Both the correlation function and IDF first calculate a function in real space from the reciprocal space intensity distribution via Fourier transform and then deduce parameters such as long spacing and lamellar height from the result. While the calculation is a straightforward process, interpretation of the data can be troublesome. For example, with IDF, crystallinities around 50% in the sample result in overlapping peaks for the height of lamellae and amorphous interlayers, which might not be properly separable. Furthermore, missing data, e.g., at low and high scattering vectors (lost due to beamstop and finite detector size) might have a noticeable influence on the result of the Fourier transform in both methods, resulting in systematic errors. We have shown before that modeling of the polymer, calculating the resulting SAXS data, and fitting of the model to the scattering patterns can foster understanding of the morphology.[10,11] Since distorting factors such as readout noise can be included in the evaluation function and since all model parameters are determined to be parallel, systematic errors in the results should be reduced and distributed on all parameters compared to methods where evaluation is a stepwise process. However, errors in the model (due to negligence of the actual morphology such as, e.g., a bimodal distribution in the long spacing)[12] will lead to completely wrong results, which might not be the case in model-free approaches such as the correlation function method.

In the present study we analyzed the structure along the lamellar stacks in a highly oriented high-density polyethylene (HDPE) film to show the benefits of our approach. HDPE is, like polypropylene or nylon, a semicrystalline polymer. Crystalline lamellae are separated by amorphous layers in the solidified state. Entanglements in the amorphous phase and tie molecules between the lamellae provide mechanical stability. Its excellent processing properties in the melt and the mechanical properties make polyethylene (PE) one of the most widely used polymers today with applications as containers, distribution pipes for gas, water, and oil, or high strength fibers.[2,13] Typical processing steps of the melt include injection molding, film blowing, melt-drawing, extrusion, or fiber spinning. In most cases, processing leads to an orientation of the chains or an elongation of the random coil, thus influencing the solidification process:[14−23] the lamellae are then oriented perpendicular to and arranged in stacks (clusters) along the drawing direction contrary to the typical spherulitic structure where the lamellae grow in the radial direction from randomly distributed nucleation points. Oriented semicrystalline polymers generally show improved mechanical and transport properties compared to their isotropic version. A detailed understanding of the morphology can therefore help to improve the materials. In our case, orientation has been achieved by melt-drawing. A special property of the used film is the high

Received: May 29, 2011
Revised: October 22, 2011
Published: October 25, 2011

optical clarity in the visible range of light. Compared to unoriented samples, the absorption coefficient is reduced by a factor of ~7−8.

Different model modifications have been tested for data evaluation, based on a two-phase structure and a one-dimensional paracrystalline lattice. We analyzed the goodness of each model and used the most suitable one to follow the structure changes during annealing and subsequent cooling of our sample to show the success of our approach.

2. MATERIAL AND METHODS

Melt-drawn HDPE film with molecular weights of M_w = 220 000 g/mol and M_n = 11 000 g/mol was provided by BASELL Polyolefine, Frankfurt, Germany. Melt-drawing was performed by unidirectional stretching of compression molded platelets (initial sheet thickness was 1 mm) at 134 °C using a biaxial stretching device (Long). For that purpose, the sheet was kept in the frame for 100 s at 134 °C and subsequently stretched at an elongation rate of 5.1 s^{-1} to a final draw ratio of 5.

Thermal properties were analyzed by differential scanning calorimetry (DSC) at a heating rate of 1 K/min under nitrogen gas flow, using a Mettler Toledo Star System (DSC1). The melting temperature T_M was taken from the minimum of the thermogram, the crystallinity was derived from the area under the DSC trace between 40 and 150 °C by relating it to the theoretical melting enthalpy of 100% crystalline PE (293 J/g).[24] We found a crystallinity of 62% and a double melting peak, located at 129.0 and 130.1 °C, respectively. The actual measurements have already been presented elsewhere[25] and we will only refer to the results retrieved there from here on.

Synchrotron SAXS measurements were performed at SSRF, Shanghai, China. The wavelength of the X-ray radiation was 0.124 nm, and the sample-to-detector distance was 5585 mm. Real-time SAXS measurements were carried out during annealing at 122 °C for 120 min and subsequent cooling to room temperature at a rate of approximately 1 K/min, using a hot stage that was available at the beamline. Each SAXS pattern was collected within 120 s.

SAXS data evaluation was performed after background correction by direct model fitting to the data in Matlab (Version 2009b; The MathWorks Inc., Natick, USA; http://www.mathworks.com). The source code is available upon request. Different models were set up and tested for this purpose. For data evaluation, we took projections of the scattering data on the meridian axis (which is the stretching direction) by integrating the intensity distribution perpendicular to it.[1]

Figure 1 shows a typical scattering pattern of the analyzed sample. We find a pattern characteristic for stretched or melt-drawn semicrystalline polymers. The crystalline lamellae are perpendicular to the stretching direction, separated by amorphous areas where noncrystallizable polymer fractions (i.e., chain ends, branches, entanglements, or other defects) are concentrated. We presented a possible model applicable to such systems before for melt-spun isotactic polypropylene (iPP).[11] There we approximated the system by assuming cylindrical crystalline domains that are arranged in a paracrystalline lattice as proposed by Hosemann.[26] In a paracrystalline lattice, distortions of the second kind are considered, meaning that the position of a lattice point only depends on the next neighbor position. This results both in lower intensities and a broadening of higher order peaks in SAXS.[11] We also introduced the possibility of orientation of those clusters/stacks toward a predefined direction (i.e., the drawing direction). With this approach, we were able to analyze

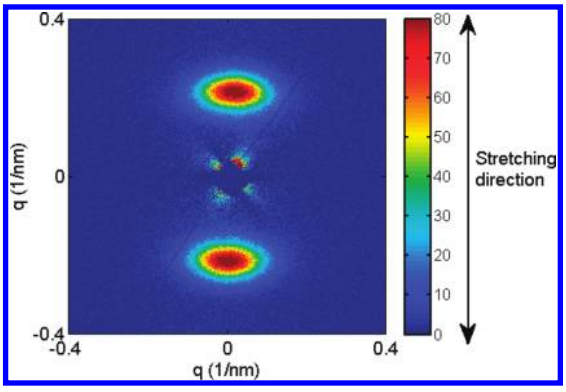

Figure 1. Typical scattering pattern of the analyzed melt-drawn HDPE sample. The stretching direction is indicated. The colorbar indicates the recorded scattering intensity.

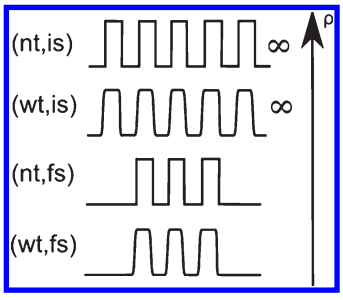

Figure 2. Density profiles of the tested models: no transition zone and infinite stack (nt,is), with transition zone and infinite stack (wt,is), no transition zone and finite stack (nt,fs), and with transition zone and finite stack (wt,fs).

long spacing of the lamellae, lamellar height, lattice distortion, lamellar radius, and degree of orientation. In the present study we will concentrate on the cluster properties along the drawing direction. As we have shown in ref 11, this can be done with a simplified model where lamellar radius and degree of orientation are not included. A first analysis with that model on the PE samples revealed that some modifications have to be implemented for better fits. We therefore tested also models where a transition zone from the lamellar to the amorphous region was included and/or a finite stack length was assumed. An overview on the different models is given in Figure 2: no transition zone and infinite stack (nt,is), with transition zone and infinite stack (wt,is), no transition zone and finite stack (nt,fs), and with transition zone and finite stack (wt,fs).

The scattering intensity of the described system is basically

$$I(q) = |F(q)\cdot T(q)|^2 \cdot (Z(q) \otimes |S(q)|^2)$$

where F denotes the scattering amplitude of the scattering objects (i.e., the lamellae), Z the lattice factor of an infinite lattice, $|S|^2$ a correction factor (shape factor) for finite cluster dimensions, applied via a convolution, and T a transition zone.[27] Assuming a rectangular density profile with a lamellar height H, the one-dimensional scattering amplitude becomes $F = \sin(qH/2)/(qH/2)$. A transition zone of width d can be introduced to the rectangular density profile in real space by folding it with a Gauss-function.[28,29] In reciprocal- or q-space, we can simply multiply the given scattering amplitude with the Fourier-transform of said Gaussian, given by $T(q) = \exp(-(dq/4)^2)$.[30]

The lattice factor of a paracrystalline lattice with a Gaussian distribution of the lattice spacing L is[26,31,32]

$$Z = \frac{1 - |h(q)|^2}{1 + |h(q)|^2 - 2|h(q)|\cos(qL)}$$

with $|h(q)| = \exp[-1/2(gqL)^2]$ where $g = \Delta L/\langle L\rangle$ (lattice distortion parameter) and $\Delta L = [\langle (L - \langle L\rangle)^2\rangle]^{1/2}$. It has been shown in literature, that the assumption of a paracrystalline lattice with lattice distortions of the second kind seem to be appropriate for semicrystalline polymers.[33,34] According to Wilke, the shape factor $|S|^2$ of a finite lattice of length NL (N being the number of long spacings per stack; for simplicity we will refer to this value as number of lamellae per stack) can be approximated by $|S|^2 = (NL)^2 \exp[-1/(4\pi)(NLq)^2]$.[30]

The free parameters of the different models of the density profile therefore are L, g, and H for no transition zone and infinite stack (nt,is), additionally d for with transition zone and infinite stack (wt,is), N for no transition zone and finite stack (nt,fs), and d and N for with transition zone and finite stack (wt,fs).

It should be noted that the presented models do not account directly for a polydispersity in the lamellar heights H. The distortion factor g only describes the lattice imperfection. We performed fits with models where polydispersity was introduced and found them to (a) increase evaluation time significantly (from seconds to several hours) and (b) tend to return with huge confidence intervals and unphysical results for the parameters (i.e., very small lamellar heights of ~1 nm with a very broad size distribution). Simulations revealed that polydispersity in H only has a significant influence on higher scattering peaks, which are barely recognizable with our samples, due to very small cluster sizes. Our tests indicated that without the assumption of polydispersity, the number of long spacings N returned by the fits of the respective models might be underestimated by one to two long spacings compared to the actual values. We assume that with "better" data, i.e., with a clear discernible second peak and a good signal/noise ratio in that scattering range, models with additional polydispersity in H would lead to even more significant results. In general, the quality of the data (especially noise) and of the preprocessing (background correction) seem to have a significant influence on the number of parameters that can be determined by a direct fitting approach. We also checked whether instrumental smearing, especially the nonzero size of the focus on the detector plane, might have an influence on the fitting process and the retrieved parameter values. Contrary to results, e.g., from colloidal dispersions and latex films,[35] where instrumental smearing can have a significant influence on the fit results, we found smearing to be negligible in the case of semicrystalline polymers.

Note that the approach to data evaluation presented here can also be used on isotropic samples after azimuthal integration and Lorentz correction.[26,34] Intermediate degrees of orientation between perfectly oriented and isotropic, however, require a more careful modeling as presented in ref 11. However, the computation time then will be significantly increased, approximately by a factor in the range of the number of data points analyzed.

3. RESULTS

As a measure for the validity of each model we compared the residuals and the goodness of fit parameters. An overview on the fits and the respective residuals is shown in Figure 3.

We find systematic deviations in the residuals, which indicate errors in the models, significantly reduced when a finite stack length is introduced (nt,is to nt,fs). The influence of the transition zone, however, seems negligible (nt,is to wt,is). It should be noted that we always find a systematic deviation at higher q values. This indicates that a minor second peak is not shown by the model calculations. As already pointed out in the description of the models this can be attributed to the lamellar height polydispersity, which has not been considered for practical reasons.

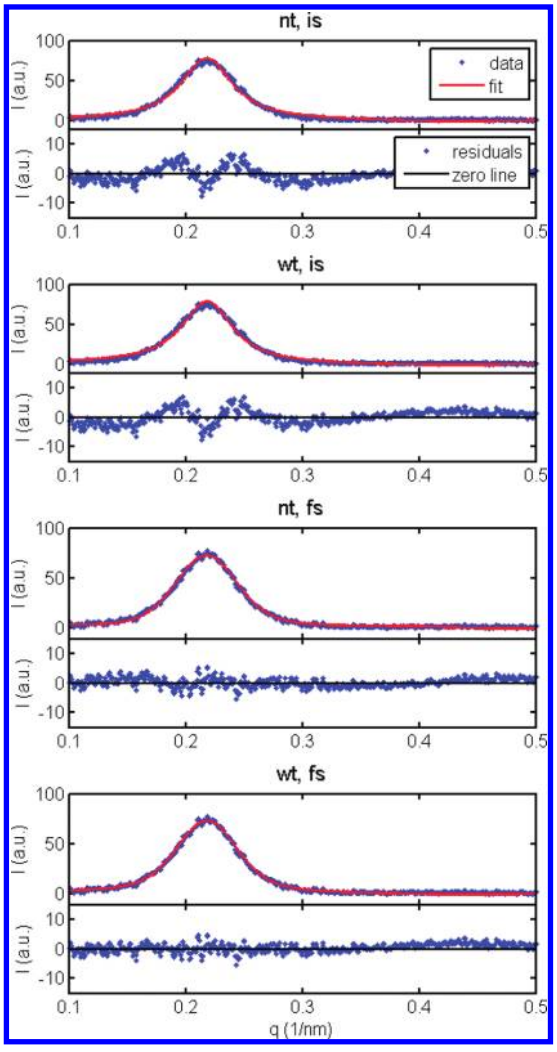

Figure 3. Fits and respective residuals achieved with the different models.

Table 1. Goodness of Fit Parameters Achieved for the Different Models

	nt,is	wt,is	nt,fs	wt,fs
ΔR^2	0.98437	0.98983	0.99355	0.99505
RMSE	2.23	1.80	1.43	1.25

Table 1 displays the goodness of fit parameters ΔR^2 (degree-of-freedom adjusted coefficient of determination) and RMSE (root mean squared error) of the given models. The "punishment" for additional parameters as included in ΔR^2 is always smaller than the reached improvement of the fits by expanding the models. As already indicated by the residual plots, we find that the introduction of a finite stack length shows the highest improvement.

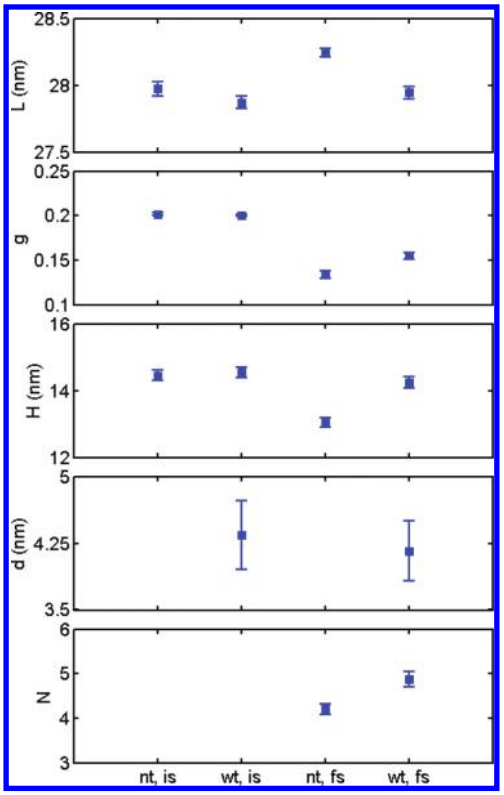

Figure 4. Resulting fit parameters for the different models.

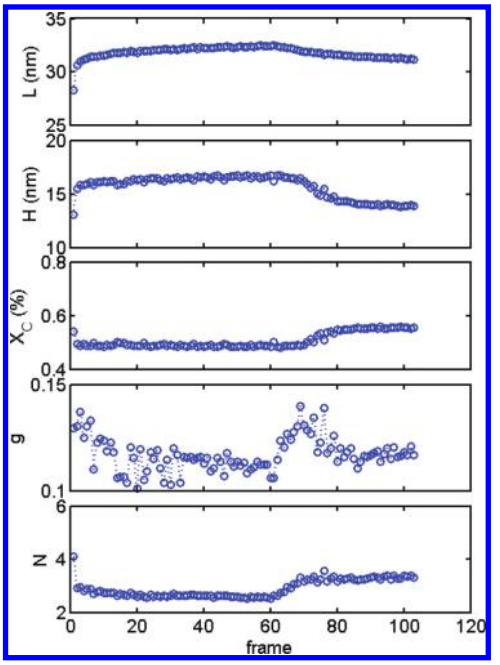

Figure 5. Overview over the retrieved model parameters during the annealing experiment. Each frame relates to 120 s of measuring time. The first frame is the room temperature measurement. After 120 min of annealing, the sample was cooled down to about 40 °C. Contrary to Figure 4, the parameter H accounts for the height of the amorphous layers due to Babinet's principle.

The resulting parameters of the fits given above are shown in Figure 4. All parameters are displayed with their 2σ confidence intervals, returned by the algorithm, as error bars. We find that the error bars quite narrow, even when more parameters are introduced. This indicates that the additional contributions are quite unique, and the parameters can be well separated from each other. The long spacing L in the given sample is about 28 nm, the width of the transition zone d is about 4.2 nm, and the number of lamellae per stack N is about 4−5. The height parameter H can describe the height of either lamellae or amorphous phase according to Babinet's principle;[2,36] therefore the crystallinity of the polymer has been determined by DSC and then compared to the SAXS crystallinity $X_C = H/L$. While the models (nt,is), (wt,is), and (wt,fs) show SAXS crystallinities of around 52%, the (nt,fs) model gives about 54% only if H is attributed to the amorphous layer. Using the 2σ confidence intervals returned by the fitting algorithm, the error in the calculated crystallinity is less than 0.7%. The measured DSC crystallinity was about 62%.[25] Therefore the (nt,fs) model seems to be the best approximation to the actual structure when using the SAXS crystallinity as a measure. The remaining difference between DSC and SAXS crystallinity can be explained by several effects: (a) DSC crystallinity is closely related to the mass fraction of crystallites. SAXS crystallinity or linear crystallinity, on the other hand, corresponds to the volume fraction of crystallites along the stack direction. Since the crystalline phase has a higher density, it is stronger weighted in DSC measurements.[2,25] A numerical calculation assuming a crystalline density of 1.000 g/cm^3 and an amorphous density of 0.855 g/cm^3 results in an ∼3.9% higher DSC crystallinity for our samples. (b) Also, it has been shown that semicrystalline polymers develop a rigid amorphous phase (RAP) where a significant part of the amorphous phase is anchored to the crystalline phase and thus restricted in molecular mobility.[37,38] The crystalline phase is therefore overestimated in DSC. (c) Additionally, single crystallites (i.e., not belonging to a stack) do not appear in SAXS. The models considering a finite stack length result in 4−5 lamellae per stack, therefore resulting in a total stack height of 110 to 140 nm. The high transparency of the melt-drawn HDPE film might be related to these lengths, which are far below the wavelengths of the visible spectrum. The lattice distortion parameter g is reduced from ∼0.2 to 0.1 when a finite stack length is included. Wilke already stated that ignoring the finiteness of stacks can be approximated by a higher lattice distortion.[30] On the other hand, the lattice distortion might be not very well defined when only 4−5 lamellae are the building blocks of one stack.

We also tested our approach on data from an annealing process that has been described before. We found the full model with transition zone and finite stack length to be troublesome during the annealing and cooling process and the retrieved parameters became unphysical (i.e., the height rather suddenly became close to 0, and the transition zone became as large as the height before). We attribute this to the rather similar contributions of transition zone and form factor to the overall scattering. Therefore we used the model where the transition zone was ignored but the finiteness of the stacks was acknowledged (nt,fs). The finiteness is the more important contribution anyway, as we have shown above. As described above, the parameter H in this context refers to the thickness of the amorphous layers when the (nt,fs) model is applied to the given measurements.

The results of the data evaluation of annealing and subsequent cooling are depicted in Figure 5; a video in avi format of the respective 2d scattering data retrieved from the detector and the fits can be found as Supporting Information to this publication. Each frame corresponds to a measuring time of 120 s with

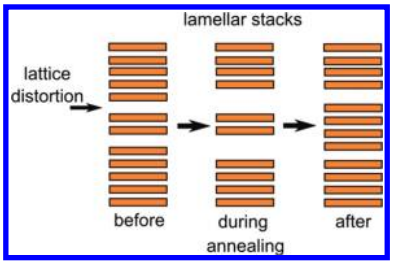

Figure 6. Model of the lamellar structure before, during, and after annealing.

exception of the first frame, which shows the results of the room temperature measurement before the annealing was started. We increased the temperature to 122 °C at a rate of 10 K/min and immediately started measurement when the final temperature was reached. After the annealing period, the sample was cooled at 1 K/min to 40 °C.

We find that the overall long spacing L increases during the heating and annealing process, mostly driven by a similar growth of the amorphous layers. The data indicate that the lamellar height in the stacks is roughly constant or grows slightly in the process. Those effects can be mainly attributed to the high thermal expansion of HDPE, which is more pronounced in the amorphous phase and a surface melting and recrystallization process.[2] SAXS linear crystallinity therefore is reduced by roughly 5% to about 50%. DSC measurements presented elsewhere on the other hand indicate that the mass crystallinity is reduced by roughly 10% at the chosen annealing temperature compared to room temperature.[25] Both results can be explained by (a) a melting of crystallites not attributed to stacks and (b) melting of lamellae at the borders of the stacks at first, which would not show directly in the SAXS results but would in the DSC measurements. This hypothesis is supported by the development of the number of lamellae per stack from roughly 4 to 3 during the heating and annealing process. We already mentioned above that since we are not considering a distribution of the lamellar thickness, the absolute number of long spacings per stack might be underestimated by 1−2. However, the general development of the stacks is not affected by this artifact. The lattice distortion is slightly reduced during annealing. This could be an effect of the reduced numbers of lamellae per stack, since now less distortion is possible (i.e., with two lamellae per stack, the lattice would be perfect regarding the considered distortions of second kind), but also of a general improvement of the lattice structure.

During the cooling process, new lamellae start to crystallize at the borders of the stacks. The number of lamellae therefore increases as does the lattice distortion. However, while the new lamellae form, their overall shape is improved as is the lattice. The distortion parameter therefore is lowered again. As a consequence, we find the overall lattice distortion improved by the annealing process compared to the room temperature measurement. During the cooling, the long spacing and amorphous height are decreasing while the SAXS crystallinity grows and finally reaches about 56%, slightly improved compared to the starting value.

We can combine the information on crystallinity X_C, stack size N, and lattice distortion g presented above into a general model on the annealing process as shown in Figure 6. Before annealing, the stacks are either rather big (five and more lamellae) or small (e.g., two lamellae). Those stacks are separated by distortions (i.e., increased amorphous regions) that are too big to attribute the lamellae to the same stack in X-ray scattering because the correlation between the lamellae is lost. In direct measurement methods such as atomic force microscopy (AFM) or transmission electron microscopy (TEM), those distortions, on the other hand, might not appear to be significant, and one would assume bigger stack sizes. During the annealing process, selective stack melting occurs at the position of the stack, separating distortions where we find an increased amount of noncrystallizable material such as chain ends, branches, and entanglements.[39] The average stack size therefore is reduced in this stage. After annealing and during cooling, we find recrystallization of lamellae in the amorphous gaps. Since the average stack size N is reduced after annealing (∼3.3) compared to the starting value (∼4.1), it appears that the newly built lamellae have to be attributed to the formerly smaller stacks: In the initial state, the scattering contribution of the smaller stacks is reduced due to their smaller scattering volume, and the average stack size appears to be higher. In the final state, the stack sizes are more uniform and contribute equally to the scattering intensity.

4. SUMMARY

We have shown that by carefully modeling the morphology of semicrystalline polymers, additional information about the structure can be obtained from SAXS experiments. Typical approaches to evaluate this kind of data are peak analysis via a Gaussian function fit, which returns a measure for the long spacing L and the lamellar height H, or the analysis of the one-dimensional correlation function with similar results. Compared to these methods, we can access morphological details such as stack size, transition zones, and lattice imperfection. Evaluating these parameters provides beneficial insight into the sample structure, especially during processing.

It turned out that especially the assumption of a finite stack length is important for improving the fits. In the given melt-drawn HDPE, usually only 4−5 lamellae contributed to one stack. Given the determined long spacing of roughly 28 nm, typical stacks have a length of 110−140 nm. Since the superstructure's (i.e., stack's) size is clearly below the wavelength of the visible spectrum, the films show a high transparency.[40]

Using the most suitable model, which considers a finite stack size, we analyzed the lamellar morphology during annealing and subsequent cooling. Although the stack size had been analyzed before, e.g., for different polymers or polymer modifications,[41,42] we are not aware of another publication where the changes in stack size and size distribution have been followed during thermal treatment. By evaluating the stack length parameter, we were able to explain the rather small changes in SAXS crystallinity during heating and annealing compared to the changes in DSC crystallinity, which is not possible with the conventional methods. More interestingly, we found a partial melting process that starts at the borders of the lamellar stacks and results in a more uniform distribution of stack sizes. Both effects do not affect the parameters long spacing and lamellar height, and therefore the SAXS crystallinity is only slightly influenced.

■ ASSOCIATED CONTENT

Supporting Information. A video containing a 2d image and respective 1d data with fit showing temperature-dependent

changes over time. This information is available free of charge via the Internet at http://pubs.acs.org.

AUTHOR INFORMATION

Corresponding Author
*E-mail: men@ciac.jl.cn.

ACKNOWLEDGMENT

We thank the National Natural Science Foundation of China (51050110442, 20734006, and 50921062) and Shanghai Synchrotron Radiation Facility project (08sr0011). S. Fischer is supported by Chinese Academy of Sciences fellowship for young international scientists (Grant No. 2010Y1GB9). We thank Dr. Hans-Friedrich Enderle and Dr. Dieter Lilge of Basell Polyolefine GmbH for providing the samples, Dr. Xiuhong Li of SSRF for assistance during SAXS experiments.

REFERENCES

(1) Stribeck, N. *X-ray Scattering of Soft Matter*; Springer: Heidelberg, 2007.
(2) Strobl, G. *The Physics of Polymers*; Springer: Berlin, 2007.
(3) Nogales, A.; Hsiao, B. S.; Somani, R. H.; Srinivas, S.; Tsou, A. H.; Balta-Calleja, F. J.; Ezquerra, T. A. *Polymer* **2001**, *42*, 5247–5256.
(4) Murthy, N. S.; Bednarczyk, C.; Moore, R. A. F.; Grubb, D. T. *J. Polym. Sci., Polym. Phys.* **1996**, *34*, 821–835.
(5) Kortleve, G.; Vonk, C. G. *Colloid Polym. Sci.* **1968**, *225*, 124–131.
(6) Vonk, C. G.; Kortleve, G. *Colloid Polym. Sci.* **1967**, *220*, 19–24.
(7) Ruland, W. *Colloid Polym. Sci.* **1977**, *255*, 417–427.
(8) Ruland, W. *Colloid Polym. Sci.* **1978**, *256*, 932–936.
(9) Stribeck, N.; Ruland, W. *J. Appl. Crystallogr.* **1978**, *11*, 535–539.
(10) Fischer, S.; Diesner, T.; Rieger, B.; Marti, O. *J. Appl. Crystallogr.* **2010**, *43*, 603–610.
(11) Fischer, S.; Marti, O.; Diesner, T.; Rieger, B. *Macromolecules* **2010**, *43*, 5009–5015.
(12) Jiang, Z.; Tang, Y.; Rieger, J.; Enderle, H.-F.; Lilge, D.; Roth, S. V.; Gehrke, R.; Heckmann, W.; Men, Y. *Macromolecules* **2010**, *43*, 4727–4732.
(13) Pasquini, N. *Polypropylene Handbook*; Carl Hanser Verlag: Munich, 2005.
(14) Schultz, J. M. *Polymer Materials Science*; John Wiley & Sons: New York, 1974.
(15) Flory, P. J. *J. Chem. Phys.* **1947**, *15*, 397–408.
(16) Samuels, R. J. *Structured Polymer Properties*; John Wiley & Sons: New York, 1974.
(17) Nakae, M.; Uehara, H.; Kanamoto, T.; Zachariades, A. E.; Porter, R. S. *Macromolecules* **2000**, *33*, 2632–2641.
(18) Uehara, H.; Nakae, M.; Kanamoto, T.; Zachariades, A. E.; Porter, R. S. *Macromolecules* **1999**, *32*, 2761–2769.
(19) Stribeck, N.; Bayer, R.; von Krosigk, G.; Gehrke, R. *Polymer* **2002**, *43*, 3779–3784.
(20) Kakiage, M.; Sekiya, M.; Yamanobe, T.; Komoto, T.; Sasaki, S.; Murakami, S.; Uehara, H. *Polymer* **2007**, *48*, 7385–7392.
(21) Kakiage, M.; Yamanobe, T.; Komoto, T.; Murakami, S.; Uehara, H. *J. Polym. Sci., Polym. Phys.* **2006**, *44*, 2455–2467.
(22) Uehara, H.; Kakiage, M.; Yamanobe, T.; Komoto, T.; Murakami, S. *Macromol. Rapid Commun.* **2006**, *27*, 966–970.
(23) Kimata, S.; Sakurai, T.; Nozue, Y.; Kasahara, T.; Yamaguchi, N.; Karino, T.; Shibayama, M.; Kornfield, J. A. *Science* **2007**, *316*, 1014–1017.
(24) Wunderlich, B. *Macromolecular Physics*; Academic Press: New York, 1973; Vol. 1.
(25) Jiang, Z.; Tang, Y.; Rieger, J.; Enderle, H.-F.; Lilge, D.; Roth, S. V.; Gehrke, R.; Wu, Z.; Li, Z.; Li, X.; Men, Y. *Eur. Polym. J.* **2010**, *46*, 1866–1877.
(26) Hosemann, R.; Bagchi, S. N. *Direct Analysis of Diffraction by Matter*; North-Holland Publishing Co.: Amsterdam, 1962.
(27) Wilke, W. *Acta Crystallogr., Sect. A* **1983**, *39*, 864–867.
(28) Vainshtein, B. K. *Diffraction of X-rays by Chain Molecules*; Elsevier Science, Ltd.: Amsterdam, 1966.
(29) Ruland, W. *J. Appl. Crystallogr.* **1971**, *4*, 70–73.
(30) Göttlicher, K.; Fronk, W.; Wilke, W. *Colloid Polym. Sci.* **1983**, *261*, 126–132.
(31) Fronk, W.; Wilke, W. *Colloid Polym. Sci.* **1983**, *261*, 1010–1021.
(32) Fronk, W.; Wilke, W. *Colloid Polym. Sci.* **1985**, *263*, 97–108.
(33) Crist, B. *J. Polym. Sci., Polym. Phys. Ed.* **1973**, *11*, 635–661.
(34) Crist, B.; Morosoff, N. *J. Polym. Sci., Polym. Phys. Ed.* **1973**, *11*, 1023–1045.
(35) Chen, X.; Fischer, S.; Yi, Z.; Boyko, V.; Terrenoire, A.; Reinhold, F.; Rieger, J.; Li, X.; Men, Y. *Langmuir* **2011**, *27*, 8458–8463.
(36) Babinet, M. *C R. Acad. Sci.* **1837**, *4*, 638–648.
(37) Sanz, A.; Nogales, A.; Ezquerra, T. A.; Lotti, N.; Munari, A.; Funari, S. S. *Polymer* **2006**, *47*, 1281–1290.
(38) Lund, R.; Alegria, A.; Goitandia, L.; Colmenero, J.; Gonzalez, M. A.; Lindner, P. *Macromolecules* **2008**, *41*, 1364–1376.
(39) Men, Y.; Rieger, J.; Strobl, G. *Phys. Rev. Lett.* **2003**, *91*, 095502.
(40) Stein, R. S.; Prud'Homme, R. *J. Polym. Sci., Polym. Lett.* **1971**, *9*, 595–607.
(41) Marega, C.; Marigo, A.; Causin, V. *J. Appl. Polym. Sci.* **2003**, *90*, 2400–2407.
(42) Marega, C.; Marigo, A.; Cingano, G.; Zannetti, R.; Paganetto, G. *Polymer* **1996**, *37*, 5549–5557.